Structure and Thermodynamics of Self-Assembled Monolayers on Gold Nanocrystallites

W. D. Luedtke and Uzi Landman*

School of Physics, Georgia Institute of Technology, Atlanta, Georgia 30332-0430

Equilibrium structures and thermodynamic properties of dodecanethiol self-assembled monolayers on small (Au$_{140}$) and larger (Au$_{1289}$) gold nanocrystallites were investigated with the use of molecular dynamics simulations. Compact passivating monolayers are formed on the (111) and (100) facets of the nanocrystallites, with adsorption site geometries differing from those found on extended flat Au(111) and Au(100) surfaces, as well as with higher packing densities. At lower temperatures the passivating molecules organize into preferentially oriented molecular bundles with the molecules in the bundles aligned approximately parallel to each other. Thermal disordering starts at $T \gtrsim 200$ K, initiating at the boundaries of the bundles and involving generation of intramolecular conformational (gauche) defects which occur first at bonds near the chains' outer terminus and propagate inward toward the underlying gold nanocrystalline surface as the temperature is increased. The disordering process culminates in melting of the molecular bundles, resulting in a uniform orientational distribution of the molecules around the gold nanocrystallites. From the inflection points in the calculated caloric curves, melting temperatures were determined as 280 and 294 K for the monolayers adsorbed on the smaller and larger gold nanocrystallites, respectively. These temperatures are significantly lower than the melting temperature estimated for a self-assembled monolayer of dodecanethiol adsorbed on an extended Au(111) surface. The theoretically predicted disordering mechanisms and melting scenario, resulting in a temperature-broadened transition, support recent experimental investigations.

1. Introduction

Materials particles of nanometer dimensions, in dispersions or in agglomerated forms (e.g., as powders, thin films, or superlattices assemblies) are of increasing interest due to the size-dependent specificity and selectivity of their physical characteristics, conferred to them by their finite size. Indeed, investigations of size-evolutionary patterns of materials properties (i.e., energetics, structure, thermodynamics, spectral, and chemical reactivity) are a principle theme in modern cluster and materials science.

Preparation of such materials often requires passivation of the individual particles to protect against modifications of their properties by their environment, as well as to inhibit their propensity to sinter. Such passivation can be achieved in various ways. One of the most elegant passivation routes is through self-assembly, that is spontaneous formation of passivating monolayers (of organic molecules such as *n*-alkylthiols), which has been shown to provide a viable means of controlling the physical and chemical properties of extended solid surfaces[1−4] and nanocrystalline facets.[5−13]

While experimental and theoretical research on self-assembled monolayers (SAMs), in particular *n*-alkylthiols chemisorbed on extended gold surfaces (Au−RS), has yielded a wealth of information,[1−4,14−16] less is known about the adsorption of such molecules on finite crystallites (which expose various crystalline facets, edges, and corner sites) and about the intermolecular organization of the molecular chains on such nanocrystallites and their thermal properties, including possible disordering and eventual melting phase transitions.[11−13,17] Furthermore, dependencies of these structural and thermodynamical properties on the size of the underlying solid nanocrystallite are expected, and they indeed have been predicted in a most recent theoretical study.[17]

In that investigation[17] the adsorption sites of dodcanethiol (C$_{12}$H$_{25}$S) and butanethiol (C$_4$H$_9$S) SAMs on small nanocrystalline gold particles exposing adjoining (111) and (100) facets (Au$_{140}$(RS)$_{62}$ and Au$_{201}$(RS)$_{80}$ with a truncated-octahedral structure motif of the gold crystallites) were studied, showing that they differ from the adsorption site geometries found on the corresponding extended gold surfaces[1,2] and that they are dependent on the size of the underlying gold nanocrystallite. Moreover, from these simulations it has been predicted that the molecules in the SAMs on such small nanocrystallites are organized into molecular bundles of preferred orientations with respect to each other, which undergo upon heating a reversible melting transition from the ordered bundled state to a uniform intermolecular orientational distribution. These transitions were found to be accompanied by intramolecular conformational changes portrayed by sharp variations in the percent trans conformations and end-to-end lengths of the molecules. The melting temperatures T_M for these SAMs were found to depend on the chain length of the passivating molecules; T_M[Au$_{140}$-(C$_{12}$H$_{36}$S)$_{62}$] = 280 K and T_M[Au$_{140}$(C$_4$H$_9$S)$_{62}$] = 160 K, which are close to (though somewhat higher than) those of the corresponding (bulk) alkyl residues, T_M(C$_{12}$H$_{26}$) = 263 K and T_M(C$_4$H$_{10}$) = 157 K.

Experimental evidence that reversible chain disordering and melting transitions occur in alkanethiolate monolayers self-assembled on gold particles had been obtained through differential scanning calorimetry (DSC),[8,11,12] and variable temperature FT-IR,[11,12] solid-state ^{13}C NMR,[11,13] and deuterium NMR[12] spectroscopies. These studies[11−13] have shown that in these systems the transition region is relatively broad (compared to gel-to-liquid crystalline transitions in liquid bilayers), and the studies noted correspondences between the thermodynamic behavior of thiolated gold nanoparticles and that of highly-

Gold Nanocrystallites

J. Phys. Chem. B, Vol. 102, No. 34, 1998 **6567**
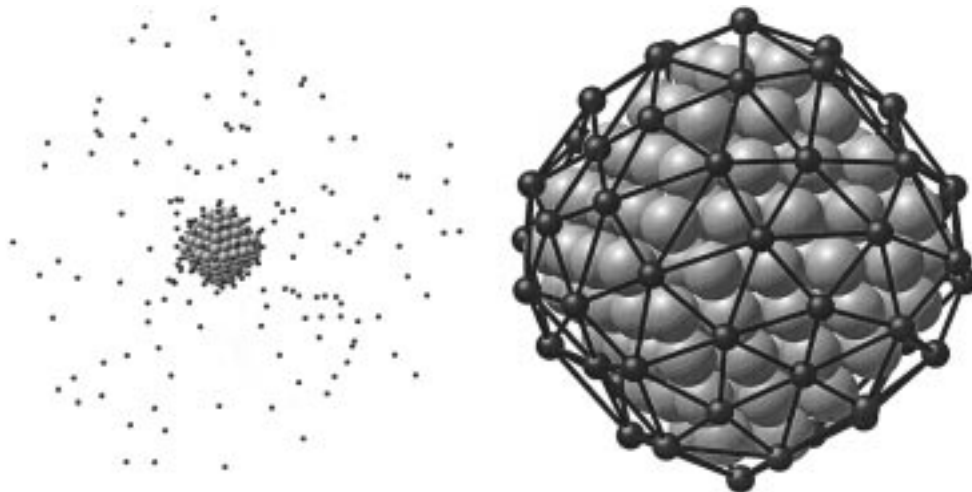
Figure 1. Left: illustration of an early stage in the preparation procedure. The Au_{140} nanocrystallite is shown surrounded by butanethiol molecules (only the sulfur atoms are depicted, as small dark spheres). Right: illustration of the compact arrangement of the thiols (only the sulfur atoms are shown) on the surface of the Au_{140} nanocrystallite at the end of the preparation process; gold atoms are depicted by larger grey spheres, and the smaller dark spheres connected by "bonds" correspond to the adsorbed sulfur atoms of the thiol molecules.

ordered two-dimensional self-assembled systems (i.e., fatty acid Langmuir–Blodgett monolayer films,[18] phospholipid bilayer membranes,[19] and electrochemical studies[20] of planar Au–RS SAMs). These observations, and the one from where formation of molecular bundles was inferred,[11] confirm our early theoretical predictions.[17] Most pertinent to our current study is a recent investigation[12] from where it was found that thermal disordering of alkanethiol monolayers on small gold particles originates at the chain terminus and propagates toward the middle of the chain as the temperature increases. Furthermore, with the use of deuterium NMR spectroscopy it has been determined that chain melting arises from an increased abundance of gauche bonds in the adsorbed alkanethiol chains.

In this investigation we study the structure and thermodynamics of alkanethiolate monolayers self-assembled on gold particles of two sizes (Au_{140} and Au_{1289}), with a focus on the thermodynamic properties and disordering and melting mechanisms of these monolayers. Following a brief description of the simulation methodology in section 2, we present our results in section 3. We summarize our findings in section 4.

2. Simulation Model

The interactions used in our molecular dynamics (MD) simulations include: (i) united-atom model potentials (non-bonded, bond-stretch, bond-angle, and dihedral terms) describing intra- and intermolecular interactions of the alkyl (CH_2 and CH_3) segments,[21] (ii) a sulfur-to-gold interatomic Morse potential[22] fitted to experimental binding energies (1.91 eV for methane thiolate, see refs 3 and 23), as well as to calculated equilibrium distances and vibrational force constants of alkyl thiolates adsorbed on Au(111) and Au(100) surfaces;[24] (iii) sulfur–sulfur and sulfur to alkyl-segment interaction potentials;[25] and (iv) an alkyl-segment to Au atom interaction potential fitted to desorption data of alkanes from metal surfaces.[26] These interaction potentials were tested by us in simulations of dodecane thiols adsorbed on extended close-packed gold surfaces, yielding results for structural and thermodynamic properties in satisfactory agreement with experimental data (that is, packing density, tilt angles, molecular conformations, melting transition, desorption energy, and mechanical response characteristics). Many-body embedded-atom potentials were employed in optimizing the structures of the bare gold clusters.[27,28]

Preparation of the passivated clusters followed the following procedure:[17] (i) the bare Au_n cluster in its optimal geometry[7,27] was surrounded by a large sphere with a reflecting boundary which was filled with butanethiol molecules in large excess compared to the number required to form a compact monolayer (see Figure 1). The system was allowed to evolve at a very low temperature, resulting in condensation of the molecules onto the cluster. (ii) The temperature was then increased to $T = 200$ K and subsequently to 300, 400, and briefly to 500 K and was cycled between these temperatures to allow desorption of excess molecules and exploration of stable binding sites. This procedure resulted in equilibrated well-annealed compact monolayers on the gold clusters (see Figure 1). (iii) The alkyl residues of the butanethiols were replaced by $R = C_{12}H_{25}$ once a compact monolayer was formed and the system was allowed to equilibrate further at 350 K (i.e., above the chain melting temperature, see section 3.ii). States of the system below (and above) this temperature were obtained by cooling (heating) the system successively and equilibrating at each temperature for long periods. We emphasize that typical equilibration times used in our simulations are rather long (e.g., $(0.5-1) \times 10^6$ integration time-steps, or 1.5–3 ns). Additionally, if the systems are not started from a high temperature configuration (in the melted-chains state, e.g., 350 K), the alkyl chains are inhibited from undergoing conformational gauche–trans barrier crossings, resulting in an inadequate exploration of the conformational phase-space within accessible MD simulations time scales and trapping in metastable nonequilibrium states. Such considerations apply to all MD simulations, and in particular to studies involving complex molecular systems (e.g., in constant pressure MD simulations of superlattices formed by thiol-passivated gold nanoclusters,[17] we found that particularly long simulations times are required (10–20 ns) in order to adequately sample the phase-space of the passivating chains, the cluster orientations, and the size and shape of the computational cell).

3. Results

i. Structures. SAMs form ordered structures on the low-index faces of extended gold surfaces;[1,2] for example,[29] the translational correlation distance in a monolayer of dodecanethiol on Au (111) is ~60 Å and on Au (100) it is 130–200 Å. The adsorption sites and packing of the thiols depend on the
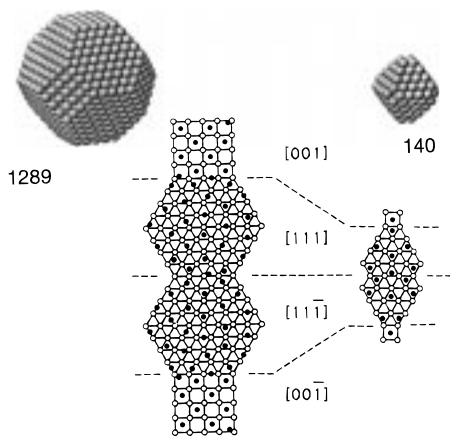
Figure 2. Arrangement of the sulfurs (filled circles) on the facets (gold atoms shown as open circles) of the equilibrium structures of Au$_{140}$(TO$^+$) and Au$_{1289}$(TO) nanocrystallites, at right and left, respectively. The corresponding structures of the bare nanocrystallites are also displayed. The nearest-neighbor distance between Au atoms is ~2.8 Å. For Au$_{140}$(C$_{12}$H$_{25}$S)$_{62}$, the inequivalent S—S distances are 3.9 and 4.5 Å (on the (111) facets) compared to a nearest-neighbor S—S distance of ~5.0 Å on an extended Au(111) surface. For Au$_{1289}$(C$_{12}$H$_{25}$S)$_{258}$, the distribution of S—S distances on the (111) facets is broad, with a peak at ~4 Å, and skewed to larger values; the average value from this distribution is 4.4 ± 0.4 Å. On the (100) facets of the nanocrystallite the average S—S distance is 4.1 ± 0.3 Å.

Au surface (calculated per molecule areas of 21.4 and 20.6 Å^2 on Au (111) and Au (100), respectively, corresponding to packing densities of 0.047 and 0.049 Å^{-2}), and the axes of the adsorbed alkyl chains are titled[1,2] with respect to the surface normal by 20—35°.

The adsorption geometry and arrangements of SAMs on finite crystalline gold nanocrystallites exposing adjacent (111) and (100) facets is further complicated. We found[17] that the arrangements of the molecules on such nanocrystallites are different from those found on extended Au surfaces and depend on the size of the nanocrystallite. In Figure 2 we show the arrangements of the sulfur atom in Au$_{140}$(RS)$_{62}$ and Au$_{1289}$-(RS)$_{258}$. For the smaller nanocrystallite[17] (whose morphology is designated[7,27] TO$^+$ indicating a truncated octahedron with the number of atoms on an edge adjoining two (111) facets m = 4, and that on an edge adjoining a (111) and a (100) facet n = 2, see cluster configurations in Figure 2) the sulfurs bind in the middle hollow site of the small (100) facets, and on the (111) facets their arrangement is hexagonally distorted with the adsorbed atoms located in the middle as well as off the hollow sites (see Figure 2, right). The sulfur arrangement occurs in two alternating inequivalent geometries on adjoining (111) facets, and the ratio of the number of gold surface atoms to adsorbed sulfur atoms is 1.55; on an extended Au(111) surface this ratio is equal to 3. On the Au$_{1289}$ nanocrystallite (with a TO morphology, $m = n = 5$), exposing much larger (100) and (111) facets (see configuration in Figure 2), the sulfurs are arranged on the (100) facets in a C(2×2) pattern occupying hollow sites, and on the (111) facets they form hexagonal nets (less distorted in the middle of the facets), with the sulfur atoms occupying mainly hollow and bridge sites with respect to the underlying gold atoms; the ratio of the number of surface gold atoms to the number of adsorbed sulfur atoms is 1.87. From these structures we find that on a spherical shell, inscribed with a mean radius of the sulfur atom positions measured from the center of the underlying gold nanocrystallite (approximately 0.9 Å larger than the mean radius of the faceted gold crystallite), the sulfur packing densities are about 30% larger than on a flat extended Au (111) surface; when referenced to the mean radius
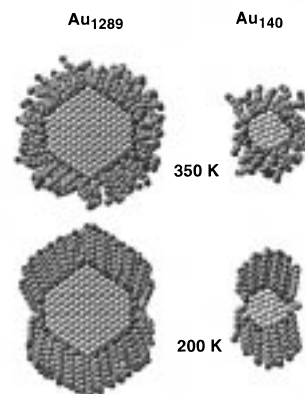

Figure 3. Equilibrium configurations of passivated Au$_{140}$(C$_{12}$H$_{25}$S)$_{62}$ and Au$_{1289}$(C$_{12}$H$_{25}$S)$_{258}$, right and left, respectively. The images were obtained via a cut through the cluster. In each case configurations are shown below (T = 200 K) and above (350 K) the chain-melting temperature. The grey spheres depict alkyl segments and the lightest ones correspond to gold atoms. Black spheres near the gold nanocrystallite correspond to sulfur atoms, and the dark grey spheres on the outside periphery depict terminal methyl groups of the dodecane thiols. Note the preferentially oriented molecular bundles at the lower temperature.

from the center of the cluster to the gold atoms on the surface the sulfur packing densities are calculated to be ~50% higher than on a planar Au(111) surface.[30]

One of the major findings in our previous investigation,[17] as well as the focus of this study, pertains to the structures and thermodynamics of the passivating monolayers. In Figure 3 we display equilibrium configurations for Au$_{140}$(C$_{12}$H$_{25}$S)$_{62}$ (on the right) and Au$_{1289}$(C$_{12}$H$_{25}$S)$_{258}$ (on the left) at low (200 K) and high (350 K) temperatures. For both cluster sizes at low temperatures, the passivating dodecanehiol molecules are "bundled" into groups of molecules with preferential "parallel" intermolecular orientations of the molecular backbones in each bundle, and the bundles themselves are preferentially oriented with respect to each other. At higher temperatures disordering and melting of the bundles occurs and the molecular configurations of the passivating monolayers transform to a uniform (with no orientational preference) structure (see Figure 3, T = 350 K). In the following we focus on the nature of these transitions.

ii. Thermodynamics. Caloric curves (total energy versus temperature) for the two passivated gold clusters, along with other characteristic properties (averages of percent trans conformations and end-to-end molecular length, R_{ee}) are shown in Figure 4, along with the corresponding results for a self-assembled dodecanthiol monolayer adsorbed on an extended flat Au (111) surface (open squares, marked Au (111) in Figure 4). For both clusters a clear signature of a phase transition is observed (see inflection points marked by arrows in the caloric curves (Figure 4). The transition (melting) temperature for the larger cluster is somewhat higher (T_M = 294 K) than that for the smaller one ($T_M \sim$ 280 K), and both are significantly lower than the measured[31] and calculated (see Figure 4) transition temperature of a dodecanethiol monolayer adsorbed on an extended Au (111) surface. As noted by us previously,[17] the melting temperatures for the monolayers passivating the gold clusters (particularly for the smaller one) are close to (somewhat higher than) that of the corresponding (bulk) alkyl residue (i.e., T_M(C$_{12}$H$_{26}$) = 263 K). The latent heat of melting of the passivating monolayers is estimated as ~20 kJ/mol (per thiol molecule) for both clusters (see Figure 4, top part).

These transitions are accompanied by intramolecular conformational changes, portrayed by sharp variations in the percent

Gold Nanocrystallites

J. Phys. Chem. B, Vol. 102, No. 34, 1998 **6569**
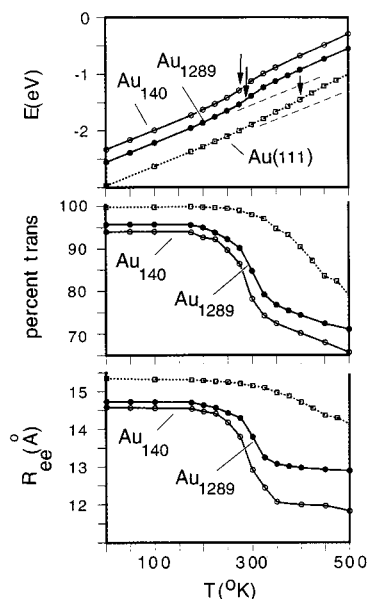
Figure 4. Caloric curves (total energy per molecule of the dodecanethiols E versus temperature T), percent trans conformations, and molecular end-to-end length (R_{ee}), top to bottom, respectively, for $Au_{140}(C_{12}H_{25}S)_{62}$ (open circles), $Au_{1289}(C_{12}H_{25}S)_{258}$ (filled circles) and for a dodecanethiol SAM on an extended Au (111) surface (open squares), respectively. The chain-melting temperatures (i.e., inflection points of the caloric curve) are denoted by arrows in the top panel. Energy, length, and temperature in units of eV, angstroms, and kelvin, respectively.

trans conformations (Figure 4, middle) and the end-to-end length (Figure 4, bottom) of the adsorbed molecules. We note here that both before and (particularly) after melting both quantities have higher (absolute) values, and the relative change in these quantities upon melting is smaller, for molecules passivating the Au_{1289} cluster. Furthermore, the corresponding (absolute) values for the molecules adsorbed on the extended Au(111) surface are significantly higher than those for the passivated clusters, and the thermally induced transitions are milder.

The melting transition of the passivating monolayers is also reflected in changes in the intermolecular structure. At low temperatures ($T < T_M$), the arrangement of molecules into bundles preferentially oriented with respect to each other (see Figure 3) is portrayed in the time-averaged normalized distributions $g(\theta)$ of the intermolecular angle between the end-to-end vectors of the thiol molecules (see $T = 1$ and 250 K in Figure 5, with the peaks near 0° and 180° indicating "antiparallel" bundles); note also the sharper peaks for the molecular bundles formed on the smaller gold cluster (Figure 5a). Above melting of the passivating layers $g(\theta)$ exhibits a broad distribution peaked about 90°, corresponding to random intermolecular orientations (see curves marked 350 K in Figure 5).

Having described above the overall structural and thermodynamic properties of the passivated gold crystallites, we discuss in the following the nature and mechanisms of the disordering and melting processes. Percent trans conformations for individual bonds of the dodecanethiol molecules passivating the Au_{140} and Au_{1289} nanocrystallites, plotted versus temperature, are given in Figures 6a and b, respectively (in each case odd-numbered and even-numbered bonds are shown in the upper and lower parts, with bond number 2 corresponding to that between the carbon atom bonded directly to the sulfur and the next outer carbon atom and bond number 11 is between the carbon bonded directly to the outer methyl group and the next inner carbon atom). We observe that (particularly prior to
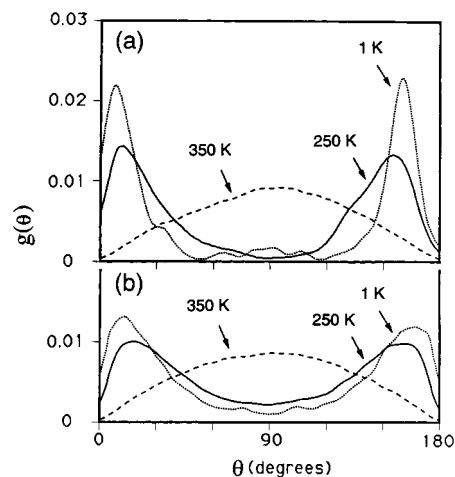

Figure 5. Normalized intermolecular angle distributions (i.e, the angle between molecular end-to-end vectors) $g(\theta)$ for $Au_{140}(C_{12}H_{25}S)_{62}$ and $Au_{1289}(C_{12}H_{25}S)_{258}$, in (a) and (b), respectively. In each case results are displayed at $T = 1$, 250, and 350 K, showing formation of molecular bundles below the chain-melting temperature. Peaks near 0° and 180° correspond to antiparallel bundles.
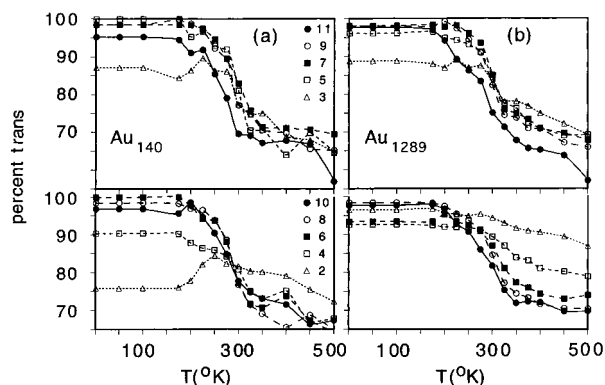
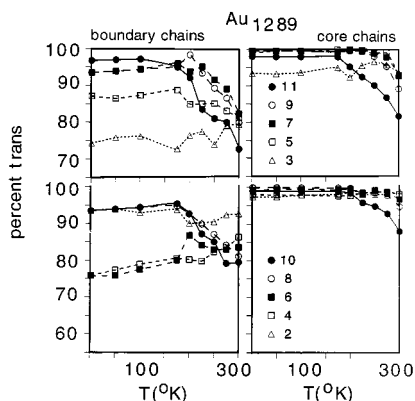**Figure 6.** Percent trans conformations in dodecane thiol SAMS on $Au_{140}(C_{12}H_{25}S)_{62}$ (in a) and $Au_{1289}(C_{12}H_{25}S)_{258}$ (in b), plotted versus temperature (in kelvin). For each case, results corresponding to odd-numbered bonds are shown in the top panel and those for even-numbered bonds are shown in the bottom one. The symbols corresponding to the various bonds are indicated. Numbering the segments in a dodecanethiol molecule 1 through 12, with segment 1 directly bonded to the sulfur atom and segment 12 the terminal methyl group; bond i denotes the one between segments i and $i + 1$.

disordering, that is, in the bundled state) the percent trans conformations of outer bonds is higher than that of inner ones (i.e., those closer to the gold nanocrystallite). This effect originates from the strain on the inner molecular bonds associated with preferentially orienting the molecules to form the molecular bundles (resulting in gauch defects) and it is particularly pronounced for the smaller nanocrystallite (e.g., see curves corresponding to bonds 2 through 5 in Figure 6a). Also noted is an alternating odd−even pattern in the values of the percent of trans conformations.

The onset of the decrease in the percent trans conformations (i.e., increase in the number of gauch defects) upon heating occurs for both nanocrystallites below the corresponding melting temperatures (see Figure 6). Most importantly, the disordering process, portrayed by the percent trans conformations, appears to initiate at outer bonds and proceed inward. Additionally, we note for some of the inner bonds of the molecules (particularly on the Au_{140} cluster) an initial increase in the percent trans conformations (see, e.g., bond 2 and 3 in Figure 6a as well as Figure 7), occurring due to thermal annealing of
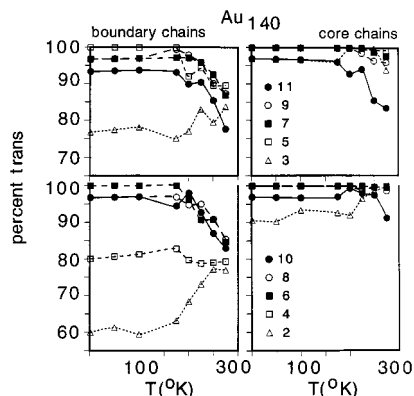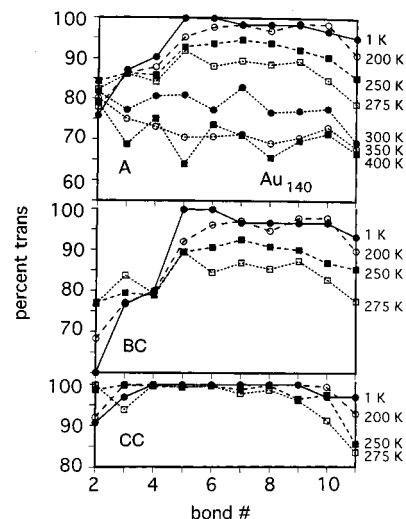
Figure 7. Percent trans conformations for boundary chains (BC) (left) and core chains (CC) (right) in $Au_{140}(C_{12}H_{25}S)_{62}$, plotted versus temperature (in degrees kelvin). For each case, results corresponding to odd-numbered bonds are shown in the top panel and those for even-numbered bonds are shown in the bottom one. The symbols corresponding to various bonds are indicated.
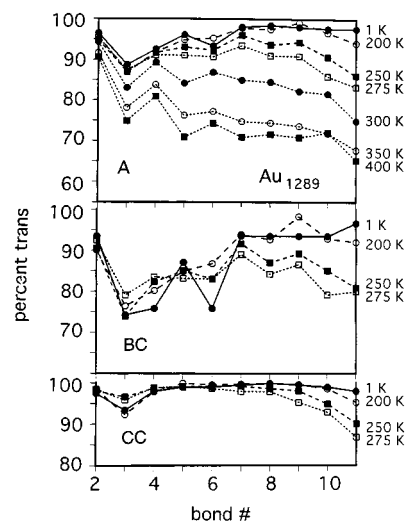

Figure 8. Same as Figure 7, but for $Au_{1289}(C_{12}H_{25}S)_{258}$.

(strain-induced) gauch defects in these bonds which is assisted by the initiation of disordering of the bundled structures. Finally, comparison of the percent trans conformations for the even-numbered bonds in the two clusters after melting indicates a significantly broader distribution of values for molecules passivating the larger nanocrystallite.

The molecules in the bundles, which form at temperatures below melting, may be classified into two groups:[32] (a) molecules which are located on the surface (outer boundary) of a bundle, which we call "boundary chains" (BC), and (b) molecules located inside the bundle, which we refer to as "core chains" (CC); the distinction between these groups of molecules is meaningful only up to the melting point. In Figures 7 and 8 we display for the molecular monolayer on the Au_{140} and Au_{1289} nanocrystallites the percent trans conformations, plotted versus T, for odd and even bonds (as in Figure 6), but separately for the BC and CC molecules. Several aspects of these distributions (particularly for the BC molecules), such as odd−even alternations and the larger propensity for gauch defects at the innermost bonds of the molecules (particularly noted for Au_{140}) are similar to those discussed above in the context of Figure 6. The main features revealed by these figures are (a) at the temperature before the onset of disordering, gauch defects (i.e., lower percent trans conformations) are significantly more abundant for the BC molecules, and (b) the BC molecules start to develop gauch defects at lower temperatures than the CC molecules. Both these observations reflect the higher structural confinement of the chains at the core of the bundles.
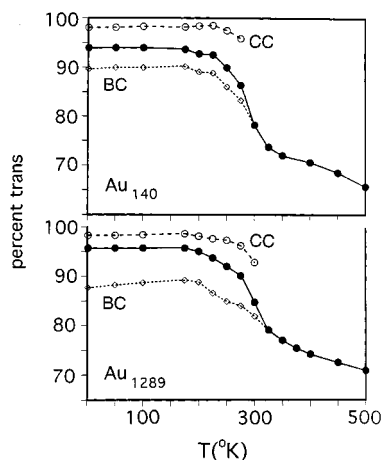

Figure 9. Percent trans conformations for $Au_{140}(C_{12}H_{25}S)_{62}$ plotted versus bond-numbers at several temperatures. Results for the whole monolayer are shown in the top panel (marked A), and separately for boundary chains (BC) and core chains (CC),in the middle and bottom panels, respectively.

Figure 10. Same as Figure 9, but for $Au_{1289}(C_{12}H_{25}S)_{258}$.

An alternative representation of the data shown in Figures 7 and 8 is given in Figures 9 and 10 where the percent trans conformations are plotted versus bond number for various temperatures; in these figures we display information pertaining to both the total percent trans conformations (upper panel, marked A) and its decomposition into BC and CC molecules. From these figures it is conveniently observed that the reduction in percent trans conformations for inner bonds (closer to the underlying gold surface) at lower temperatures (particularly pronounced for the passivating molecules on the Au_{140} nanocrystallite, see Figure 9) originates mainly from the boundary chains of the bundles (compare middle and bottom panels in Figures 9 and 10), which undergo a larger distortion (resulting in gauch defects) in the course of formation of the oriented bundles. It is also seen that the disordering (expressed as decrease in percent trans conformations) starts at temperatures below melting and proceeds from the outer bonds inward (though even inner bonds undergo conformational changes at these temperatures, but prior to melting these changes are smaller than those occurring at the outer bonds). Finally we note (particularly for the Au_{1289} nanocrystallite where larger facets are exposed) that in the melted state of the overlayers

Gold Nanocrystallites

J. Phys. Chem. B, Vol. 102, No. 34, 1998 **6571**

Figure 11. Percent trans conformations in $Au_{140}(C_{12}H_{25}S)_{62}$ (top) and $Au_{1289}(C_{12}H_{25}S)_{258}$ (bottom) plotted versus temperature (in kelvin). In each case results are shown for the whole monolayer (filled circles) and separately for the core chains (CC, empty circles) and boundary chains (BC, diamonds).

odd−even alternations occur predominantly for inner bonds (see in particular top panel in Figure 10 for $T \geq 275$ K).

A summary of the results pertaining to the melting of boundary and core molecules on the two clusters is given in Figure 11 illustrating (a) that at low temperatures BC molecules are characterized by smaller percent trans conformations than molecules in the core of the bundles, and (b) that disordering initiates for molecules at the bundles' boundary, propagating into the bundles' core region as the temperature increases toward melting.

4. Summary

We investigated here, with the use of molecular dynamics simulations, the equilibrium structures and thermodynamic properties of self-assembled monolayers of dodecanethiol on gold nanocrystallites. To explore dependencies on the size of the underlying metal cluster studies were performed for SAMs on Au_{140} and Au_{1289}, with both bare clusters having a face-centered cubic crystalline structures with truncated octahedral morphologies (see Figure 2).

In the passivated forms of $Au_{140}(C_{12}H_{25}S)_{62}$ and $Au_{1289}(C_{12}H_{25}S)_{258}$, the thiol molecules adsorb on the (111) and (100) nanocrystalline facets to form compact monolayers (Figures 1−3). The adsorption site geometries on the nanocrystallites (Figure 2) differ from those found on extended flat Au(111) and Au(100) surfaces. The SAMs on the nanocrystallites are characterized by larger packing densities, that is, ratios of 1.55 and 1.87 between the number of exposed surface gold atoms to the numbers of adsorbed sulfur atoms for the smaller and larger nanocrystallites, respectively, compared to a ratio of 3 for a dodecanethiol SAM on Au(111). At lower temperatures the passivating molecules organize into molecular bundles preferentially aligned with respect to each other in a close to antiparallel manner, with the backbones of the molecular chains in the bundles packed approximately parallel to each other in order to maximize their intermolecular (nonbonded) interactions (see Figures 3 and 5). The molecules in each bundle may be divided into two groups: core chains (CC) at the inside, and boundary chains (BC) on the surface of the bundle. Alignment of the BC molecules in the bundles is accompanied by strain which generates gauche defects at intramolecular bonds close to the surface of the underlying gold nanocrystallite (see Figures 7 and 8).

Thermal disordering of the bundles starts to occur at $T > 200$ K (Figures 4 and 6) culminating in melting of the bundled structures into a uniform distribution of the chains around the gold nanocrystallite (Figure 5). Melting of the passivating monolayers, determined from the inflection point in the caloric curve, occurs at $T_M[Au_{140}(C_{12}H_{25}S)_{62}] = 280$ K and $T_M[Au_{1289}(C_{12}H_{25}S)_{258}] = 294$ K, which are significantly lower than the temperature of a dodecanethiol SAM on an extended Au(111) surface, and closer to, though higher than, the melting temperature of the corresponding (bulk) alkyl residue ($T_M(C_{12}H_{26}) = 263$ K).

Disordering of the monolayers initiates at the bundles' surfaces (i.e., involving BC molecules (Figures 7−11)). Except for initial annealing of the aforementioned strain-induced conformational (gauche) defects (for inner bonds of BC molecules), the disordering process for both BC and CC molecules involves generation of gauche defects, occurring first at bonds between the terminal molecular segments near the outer surface of the passivating monolayer and then propagating with increasing temperature inward toward the gold surface (Figures 6−8). This mechanism supports recent results obtained from variable temperature deuterium NMR studies.[12] The predicted distribution of disordering temperatures due to variations in the coordination and intermolecular interactions of boundary and core chains in the bundles and the sequential propagation with increasing temperature of thermal-induced disorder from the molecular chain terminus toward the surface of the underlying gold nanocrystallite are reflected in broadening of the melting transition of SAMs on finite crystallites, as observed experimentally.[11−13]

Finally, we remark that the organization of the SAM molecules on the nanocrystallites into molecular bundles occurs not only for isolated passivated clusters but also when they form three-dimensional superlattices.[17] Moreover, the bundled geometry affects the structure of the superlattice (e.g., via interlocking of the molecular bundles[17,33]) and its thermodynamic properties. These issues pertaining to condensed phases of passivated nanocrystalline materials are the subject of continuing investigations in our laboratory.[34]

References and Notes

(1) Ulman, A. An Introduction to Ultrathin Organic Films; Academic Press: San Diego, CA, 1991.

(2) Ulman, A. *Chem. Rev.* **1996**, *96*, 1533 and references therein.

(3) Dubois, L. H.; Nuzzo, R. G. *Ann. Rev. Phys. Chem.* **1992**, *43*, 437. Nuzzo, R. G.; Allara, D. L. *J. Am. Chem. Soc.* **1983**, *105*, 4481.

(4) Terrill, R. H.; et al. *J. Am. Chem. Soc.* **1995**, *117*, 12537 and references therein. Also see: Fenter, P.; Eberhardt, A.; Eisenberger, P. *Science* **1994**, *266*, 1216 and references therein.

(5) Brust, M.; Walker, M.; Bethell, D.; Schriffin, D. J.; Whyman, R., *J. Chem. Soc., Chem. Commun.* **1994**, 801.

(6) Brust, M.; Bethell, D.; Schriffin, D. J.; Kiely, C. J. *Adv. Mater.* **1995**, *7*, 795.

(7) Whetten, R. L.; Khoury, J. T.; Alvarez, M.; Murthy, S.; Vezmar, I.; Wang, Z. L.; Stephens, P. W.; Cleveland, C. L.; Luedtke, W. D.; Landman, U. *Adv. Mater.* **1996**, *8*, 428. Whetten, R. L.; et al. In *Chemical Physics of Fullerenes 5 and 10 Years Later*; Andreoni, W., Ed.; Kluwer: Dordrecht, 1996. Schaaff, T.; Shafigulin, M.; Khoury, J.; Vezmar, I.; Whetten, R. L. *J. Phys. Chem.* **1997**, *101*, 7886.

(8) Terrill, R. H.; et al. *J. Am. Chem. Soc.* **1995**, *117*, 12537.

(9) O'hara, P. C.; Leff, D. V.; Heath, J. R.; Gelbart, W. M. *Phys. Rev. Lett.* **1995**, *75*, 3466.

(10) Dorogi, M.; Gomez, J.; Osifchin, R.; Andres, R. P.; Reifenberger, R. *Phys. Rev. B* **1995**, *52*, 9071.

(11) Badia, A.; Singh, S.; Demers, L.; Cuccia, L.; Brown, G. R.; Lennox, R. B. *Chem. Eur. J.* **1996**, *2*, 359.

(12) Badia, A.; Cuccia, L.; Demers, L.; Morin, F.; Lennox, R. B. *J. Am. Chem. Soc.* **1997**, *119*, 2682.

(13) Badia, A.; Gao, W.; Singh, S.; Demers, L.; Cuccia, L.; Reven, L. *Langmuir* **1996**, *12*, 1262.

(14) Hautman, J.; Klein, M. L. *J. Chem. Phys.* **1989**, *91*, 4994.

(15) Hautman, J.; Klein, M. L. *J. Chem. Phys.* **1990**, *93*, 7483.

(16) Mar, W.; Klein, M. L. *Langmuir* **1994**, *10*, 188 and references therein.

(17) Luedtke, W. D.; Landman, U. *J. Phys. Chem.* **1996**, *100*, 13323.

(18) Rieglar, J. E. *J. Phys. Chem.* **1989**, *93*, 6457.

(19) Marsh, D. *Handbook of Lipid Bilayer Membranes*; CRC Press: Boca Raton, 1991; pp 135−150.

(20) Badia, A.; Back R.; Lennox, R. B. *Angew. Chem., Int. Ed. Engl.* **1994**, *33*, 2332.

(21) Jorgensen, W. L.; Madura, J. D.; Swenson, C. J. *J. Am. Chem. Soc.* **1984**, *106*, 6638. Supplemented by angle-bending potentials following Ploeg, P.; Berendsen, H. J. C. *J. Chem. Phys.* **1982**, *76*, 3271.

(22) The bonding interaction between a sulfur atom and the gold atoms was modeled by us[17] via a pairwise additive Morse potential, $U(r) = \epsilon \exp(-\beta(r - r_m))[\exp(-\beta(r - r_m)) - 2]$, with $\epsilon = 0.4$ eV, $\beta = 1.3$ Å^{-1}, $r_m = 2.9$ Å, and the potential was shifted by a constant offset so that it goes smoothly to zero at a cutoff radius $R_{cut} = 5.8$ Å. The parameters which we determined are close to those determined independently by Mahaffy, R.; Bhatia, R.; Garrison, B. J. *J. Phys. Chem. B* **1997**, *101*, 771.

(23) Nuzzo, R. G.; Zegarski, B. R.; Dubois, L. H. *J. Am. Chem. Soc.* **1987**, *109*, 733.

(24) Sellers, H.; Ulman, A.; Shnidman, Y.; Eilers, J. E. *J. Am. Chem. Soc.* **1993**, *115*, 9389.

(25) Jorgensen, W. L. *J. Phys. Chem.* **1986**, *90*, 6379 (with modifications similar to those in ref 14; Jorgensen's Lennard-Jones pair-potential parameters with combining rules were used, except for the sulfur−sulfur distance parameter taken by us as $\sigma_{ss} = 4.45$ Å which stabilizes the equilibrium S−S adsorption geometry on an extended flat Au(111) surface).

(26) Xia, T. K.; Ouyang, J.; Ribarsky, M. W.; Landman, U. *Phys. Rev. Lett.* **1992**, *69*, 1967.

(27) The optimal structures of the gold cores were taken as those determined through simulations of bare gold clusters. Mass spectrometry, transmission electron miccroscopy, and X-ray measurements performed on isolated fractions of solution-phase prepared passivated gold crystallites confirmed that the structures of the gold cores of dodecanethiol passivated clusters are the same as those predicted in the simulations. See: ref 7; Cleveland, C. L.; Landman, U.; Shafigullin, M.; Stephens, P. W.; Whetten, R. L. *Z. Phys. D* **1997**, *40*, 282.

(28) The parameterization used is after Adams, J. B.; Foiles, S. M.; Wolfer, W. G. *J. Mater. Res.* **1989**, *4*, 102.

(29) Strong, L.; Whitesides, G. M. *Langmuir* **1988**, *4*, 546.

(30) A similar result has been reached on the bais of geometric arguments and elemental analysis in ref 5; see also an estimate based on a simple model in Leff, D. V.; Ohara, P. C.; Heath, J.; Gelbart, W. M. *J. Phys. Chem.* **1995**, *99*, 7036.

(31) Fenter, P.; Eisenberger, P.; Liang, K. L. *Phys. Rev. Lett.* **1993**, *70*, 2447.

(32) To distinguish between molecules in the core and boundary regions of the molecular bundles we calculated for each of the molecules the average (per chain) two-body nonbonded interactions between its segments and those of all the other molecules. For the bundled state the distribution of these intermolecular interaction energies is bimodal reflecting variations in the packing and coordination of the molecules; the boundary chains (BC), having roughly half the number of nearest neighbor chains compared to the fully coordinated chains at the core of the bundle, are characterized by higher (less negative) potential energy values. Therefore, molecules contributing to the higher energy component of the bimodal intermolecular interaction energy distribution were assigned as BC molecules and the other chains as belonging to the core (CC) of the bundle. Obviously, this distinction is valid only as long as the molecular bundle state maintains; for temperatures close to melting the high degree of disordering results in a broad energy distribution and the distinction between BC and CC molecules is not useful.

(33) For an experimental confirmation of the predictions pertaining to bundling given in ref 17, see Wang, Z. L.; Harfenist, S. A.; Whetten, R. L.; Bentley, J.; Evans, N. D. *J. Phys. Chem. B* **1998**, *102*, 3068.

(34) Luedtke, W. D.; Landman, U., to be published. We note that in superlattices, bimodal bundles may form, as well as arrangements involving several oriented molecular bundles due to the more complex intercluster molecular packing constraints.